Multiphoton Lithography of Nanocrystalline Platinum and Palladium for Site-Specific Catalysis in 3D Microenvironments

Lauren D. Zarzar,[†] B. S. Swartzentruber,[‡] Jason C. Harper,[§,||] Darren R. Dunphy,[§] C. Jeffrey Brinker,[§,||] Joanna Aizenberg,*,[†,⊥,#] and Bryan Kaehr*,[§,||]

[†]Department of Chemistry and Chemical Biology, Harvard University, Cambridge, Massachusetts 02138, United States

[‡]Center for Integrated Nanotechnologies, Sandia National Laboratories, Albuquerque, New Mexico 87106, United States

[§]Department of Chemical and Nuclear Engineering and Center for Micro-Engineered Materials, University of New Mexico, Albuquerque, New Mexico 87206, United States

[||]Advanced Materials Laboratory, Sandia National Laboratories, Albuquerque, New Mexico 87106, United States

[⊥]School of Engineering and Applied Sciences, Harvard University, Cambridge, Massachusetts 02138, United States

[#]Wyss Institute for Biologically Inspired Engineering, Harvard University, Cambridge, Massachusetts 02138, United States

S *Supporting Information*

ABSTRACT: Integration of catalytic nanostructured platinum and palladium within 3D microscale structures or fluidic environments is important for systems ranging from micropumps to microfluidic chemical reactors and energy converters. We report a straightforward procedure to fabricate microscale patterns of nanocrystalline platinum and palladium using multiphoton lithography. These materials display excellent catalytic, electrical, and electrochemical properties, and we demonstrate high-resolution integration of catalysts within 3D defined microenvironments to generate directed autonomous particle and fluid transport.

Platinum and palladium catalysts are crucial for a broad range of existing and emerging chemical, biological, and technological applications. Consequently, substantial recent work has been aimed at understanding and improving their function and efficiency and reducing their consumption/ utilization via nanostructuring.[1] Despite progress toward directed synthesis of a wide variety of platinum and palladium nanostructures and alloys, there are few reported strategies for integration of these catalysts within nano or microscale platforms. Specifically, abilities to dictate catalysis within microfluidic systems are crucial for the success of lab on chip devices which rely on well-defined catalyst/substrate interactions for improved efficiency, portability, and cost.[2] Increasingly microfluidic designs incorporate 3D channel geometries,[3,4] and therefore development of a strategy for precise positioning of catalysts within 3D microfluidics should prove enabling for a wide range of technologies, including autonomously powered microfluidics, diagnostics, microreactors, and sensors as well as energy generation, conversion, and storage applications.[5−7]

Platinum, palladium, and rhodium have been incorporated into microfluidic hydrogenation reactors using procedures such as sputtering,[8,9] and recently Xu et al. used direct laser writing to pattern catalytic and surface enhanced Raman spectroscopy (SERS)-active silver microflowers within a microfluidic
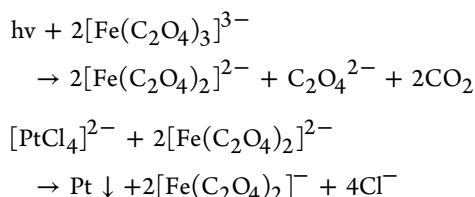
channel.[10] Despite these examples, the scope of catalyst printing for microreactors remains limited, and successful integration of catalysts, such as Pt and Pd, within 3D microfluidics has not been demonstrated.

Here we describe a straightforward procedure to integrate arbitrary micropatterns of nanostructured Pt and Pd within 3D fluidic architectures using multiphoton lithography (MPL), an intrinsically 3D direct-write technique.[11,12] These MPL-deposited Pt and Pd materials are composed of polycrystalline metallic nanoparticles that show excellent electronic, electrochemical, and catalytic properties. We show that site-specific H_2O_2 decomposition catalyzed by MPL-directed Pt can be used to drive directed fluid flow in three dimensions upon integration within appropriately designed 3D structural components, which we envision can be applied broadly for site-specific catalysis in microfluidic environments, for instance, toward the design and testing of catalytic micropumps and motors.[13−17]

The use of MPL to form conductive metallic structures has been explored,[18−21] however, reports on MPL of catalytic materials are scant,[10,22] and the use of MPL to form Pt and Pd materials has not been reported. Previously, photoreduced Pt and Pd nanomaterials have been synthesized using methods often requiring the use of chemical stabilizers in order to generate nanoparticles or nanowires.[23−26] To adapt the synthesis of Pd and Pt nanocrystals for MPL conditions, we explored the use of precursors often used in platinotype/ palladiotype photographic processes first developed in the late 19th century[27] and recently adapted by Jiang and Miller for fuel cell applications.[28,29] In one such printing method, paper (serving as the support matrix) is embedded with $(NH_4)_2[PtCl_4]$ or $(NH_4)_2[PdCl_4]$ and $(NH_4)_3[Fe(C_2O_4)_3]$ and exposed to UV light, inducing photochemical reduction of

the iron to form a strong reducing agent which can then reduce, for instance, Pt(II) to Pt(0) in the following reactions:

$$hv + 2[Fe(C_2O_4)_3]^{3-}$$
$$\rightarrow 2[Fe(C_2O_4)_2]^{2-} + C_2O_4^{2-} + 2CO_2$$

$$[PtCl_4]^{2-} + 2[Fe(C_2O_4)_2]^{2-}$$
$$\rightarrow Pt \downarrow + 2[Fe(C_2O_4)_2]^{-} + 4Cl^{-}$$

To investigate MPL of Pt and Pd through adaption of this photographic process, we mixed a 1:1 volume precursor solution comprised of 0.7 M of either the $(NH_4)_2[PtCl_4]$ or the $(NH_4)_2[PdCl_4]$ and 1.0 M of the iron(III) oxalate and tested Pt/Pd direct-writing using a mode-locked titanium:sapphire laser centered at 750 nm and focused upon a glass coverslip [Supporting Information (SI)]. Using a scanning laser, dynamic mask-based approach,[12] arbitrary Pt and Pd patterns could be printed on unmodified glass (Figure 1a).
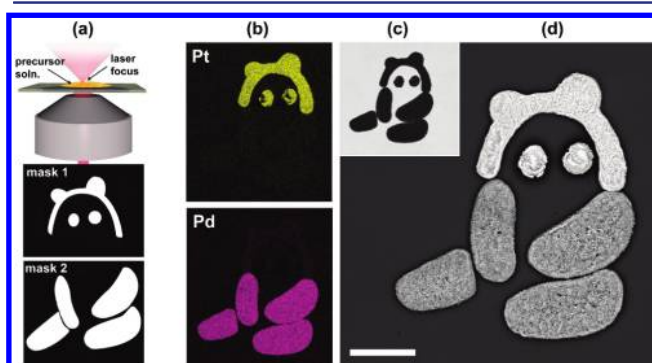

Figure 1. (a) Fabrication schematic showing the two digital masks used to define Pt and Pd. (b) EDS image maps indicating regions of Pt and Pd. (c) Bright-field optical micrograph. (d) Backscatter SEM. Scale bar, 20 μm.

Bubbles were observed emanating from the opaque structure at the point of laser focus/fabrication, indicating solution boiling with likely contribution of CO_2 evolution from ferric oxalate reduction (movie 1, SI). Structures could be rinsed rigorously without any detectible delamination or degradation. Figure 1b,d shows energy-dispersive X-ray spectrographs (EDS) and backscatter scanning electron micrographs (SEM), respectively, demonstrating the fabrication of well-defined patterns of highly pure (i.e., no iron oxide contaminant detected with EDS) Pt and Pd.

The $(NH_4)_2[PtCl_4]$, $(NH_4)_2[PdCl_4]$, and $(NH_4)_3[Fe(C_2O_4)_3]$ precursors display no significant absorbance above ~550 nm (Figure S1, SI),[27] and excitation of the charge-transfer band of $[Fe(C_2O_4)_3]^{3-}$, which is required for its subsequent photolysis, is achieved in the range of ~200−500 nm.[30,31] Thus, as expected, no initial deposition was observed when 5 mW continuous wave (CW) 750 nm light was employed indicating a multi-photon absorption process is required for initiation. High-resolution SEMs (Figure 2a,b) show that the metallic patterns are comprised of small metallic granules, indicating that the rate of photoreduction within the focal volume is limited by the diffusion of metallic precursors.[32−34] SEM cross-sectional analysis of an representative Pd structure revealed that the granular surface, in large part, is continuous throughout the structure interior down to the glass/metal interface, at which point the structure appears
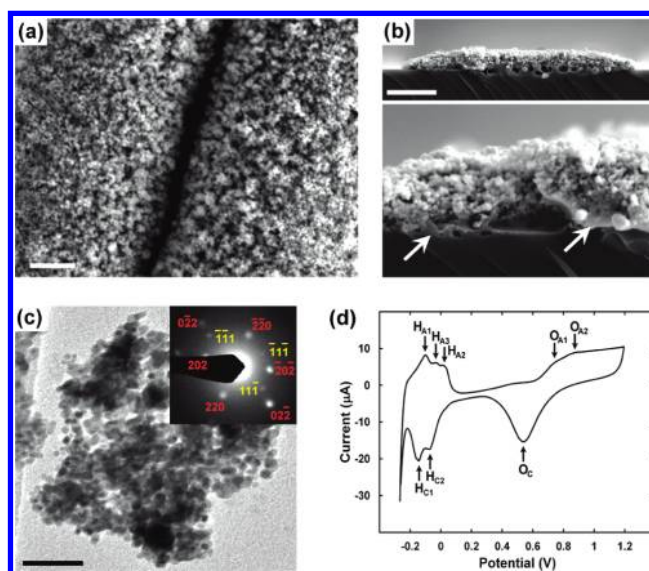

Figure 2. (a) Two Pd structures separated by a ~200 nm gap. Scale bar, 1 μm. (b) Cross section of a MPL-Pd line showing melting/annealing of the glass (left arrow) and Pd (right arrow). Scale bar, 5 μm. (c) TEM of MPL-Pt crystallites and electron diffraction pattern obtained from the edge of a cluster (corresponding to two crystallites). Scale bar, 50 nm. (d) CV of an MPL-Pt working electrode in 1.0 M H_2SO_4 shows hydrogen adsorption (cathodic peaks; H_C) and desorption (anodic peaks; H_A) and formation ($O_{A1,2}$) and subsequent reduction (O_C) of an oxide layer.

solidified, indicating thermal melting/annealing at the interface (Figure 2b)—a consequence of heating via light absorption by the metallic pads. We estimated the steady-state temperature rise (ΔT) at the laser focal point of the glass/metal interface using the solution for the low-frequency limit (essentially CW) of the laser modulation:[35]

$$\Delta T = \frac{A_0}{2\sqrt{\pi}\, w_0 \Lambda}$$

where A_0 is the average power (~5 mW) multiplied by the percentage of light absorbed by the metal at 750 nm (~30% for Pt and Pd), w_0 is the $1/e^2$ radius of the focused laser spot (~350 nm), and Λ is the thermal conductivity of the glass (1.3 W m^{-1} K^{-1}) giving a maximum steady-state temperature rise of ~930K under these conditions, which is substantially higher than the annealing point of the borosilicate cover glass (557 °C).[36] Interestingly, we observed that further deposition of chemically and structurally identical Pt or Pd could be extended from an existing metallic structure using 750 nm CW laser light and the same precursor solutions whereas structures could not be deposited in this manner in the absence of the iron sensitizer. These observations indicate that the heat generated at the point of focus at the glass/metal interface leads to localized thermal decomposition/reduction of the ferric oxalate into an iron(II) reducing agent. The mechanism of metal oxalate thermal decomposition and resulting intermediates is highly dependent on experimental and environmental conditions,[37] but extensive heating can result in the reduction of iron(III) to iron(II) with FeC_2O_4 as a possible intermediate.[38] FeC_2O_4 has also been shown to reduce platinum and palladium precursors salts.[27] Moreover, this mechanism provides an avenue to explore direct writing of metals using widely available and less costly CW light sources.

Using our direct write setup, we observed a reproducible minimum line width of ca. 2 μm, with gap width resolutions of ca. 200 nm (Figure 2a).[39] We characterized the electrical properties of MPL-Pt and -Pd lines written on glass substrates using an in situ nanoprobe technique (Figure S2, SI) and measured resistivity values of 4.2 ± 0.5 and 2.3 ± 0.3 ($\mu\Omega$ m) for Pt and Pd, respectively, which is approximately 1 order of magnitude higher than those for bulk metals. Further characterization of the crystallinity and electrochemical properties of MPL-Pt was carried out using transmission electron microscopy (TEM). TEM analysis of the MPL-deposited Pt scraped from glass substrates showed clusters with crystallites ranging in diameter from 4 to 8 nm (Figure 2c), and distinct crystallographic planes could be resolved in the electron diffraction pattern of crystallites located at cluster edges (Figure 2c inset). Cyclic voltammetry (CV) was used to characterize MPL-Pt (Figure 2 and Figure S3, SI), and we measured an electroactive surface area to geometric surface area ratio of ∼36.

The emerging field of synthetic catalytic nanomotors and pumps provides an exciting testbed to explore nanomaterials with life-like energy conversion strategies.[5−7,40] To achieve the work necessary to directionally power such devices generally requires asymmetric placement of the catalyst in relation to the surrounding environment in order to generate net directional motion and flow.[14−17,41] MPL enables arbitrary 3D structures to be readily designed and fabricated allowing functional/ asymmetric geometries to be rapidly prototyped. We explored Pt-catalyzed decomposition of H_2O_2 to generate directed fluid and particulate flow within 3D microchambers and channels. In Figure 3a, a Pt pad was patterned onto glass and then encased within a photocross-linked protein chamber containing a self-crossing spiral outlet. Addition of 1% H_2O_2 resulted in continuous and directed flow of oxygen through the spiral (movie 2, SI), as the peroxide substrate could be replenished at the catalytic site, for the most part, via diffusion across the protein hydrogel chamber walls and ceiling thereby allowing the majority of the spiral channel to maintain constant O_2 pressure. In contrast, directing the oxygen outflow into an asymmetric channel (Figure 3b) resulted in a peristalsis-like effect on the channel, with the channel fluid periodically compressed and released by the oxygen bubble evolution and resultant negative pressure developed upon outflow. Pumping is illustrated by the directional transport of microspheres at relatively high velocities (up to ca. 60 μm s^{-1}) through the channel (Figure 3b and movie 3, SI). Importantly, this approach offers greater flexibility versus existing techniques[15,17] in the design of autonomously powered microfluidics.

Finally, we explored Pt patterning within a preformed 3D microenvironment. Unfortunately, formation of metallic pads on protein substrates resulted in deformation of the protein support. However, this challenge was overcome by developing a silica composite[42] which provided sufficient mechanical reinforcement of the structural surfaces defined by the protein template to withstand the subsequent heat generated during metal deposition. We designed a geometry where gas flow is forced downward, underneath the catalyst, to exit into the surrounding fluid (Figure 3c). Traversing the imaging plane through the structure shows that the gas generated from the top chamber is directed underneath the Pt catalyst (movie 4, SI), demonstrating high-resolution integration of a metallic component that is otherwise unachievable without 3D lithographic control.
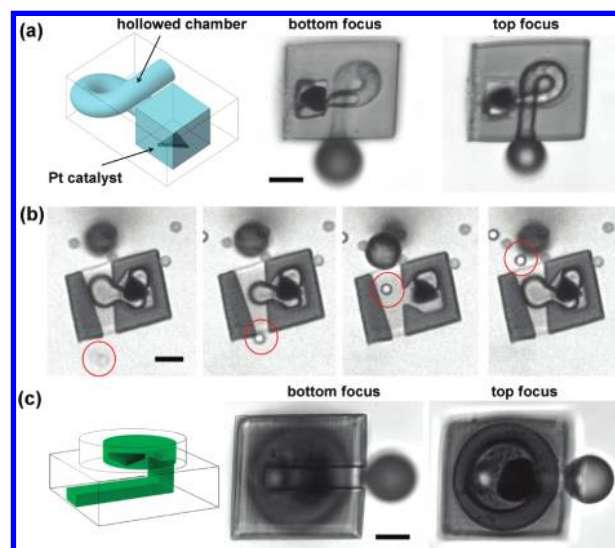

Figure 3. (a) A Pt catalyst contained in a protein chamber directs gas through a self-crossing spiral channel. (b) The directional outflow of gas produced at an MPL-Pt catalyst contained in a microchamber pumps a 5 μm particle (circled in red) through the asymmetric channel over approximately 1 s. (c) An MPL-Pt catalyst printed inside the upper chamber of a 3D microchamber directs gas flow downward underneath the catalyst. Scale bars, 10 μm.

We have demonstrated that MPL of Pt and Pd facilitates the design of dynamic microsystems based on harnessing localized catalysis within 3D microenvironments to generate directed fluid and gas flow. These autonomous pumps and fluidics may be useful for flow generation, fluid mixing, propulsion, collection, and transport. Additionally MPL-Pt and -Pd materials display excellent electronic and catalytic functionality; further enhancement is expected by exploring alloyed systems and controlling resolution and particle morphology using structure-directing agents[1,32,43,44] or electroplating techniques.[45] Fabrication of Pt and Pd structures with free-form, 3D architectures is currently being investigated through judicial variation of the chemical and environmental parameters in an effort to overcome the low structural fidelity incurred via laser heating.[18,19,32] The ability to prototype arbitrary 3D microscale electroactive and catalytic surfaces provides a new toolset with which to fabricate dynamic, 3D nano and microscale systems.

■ ASSOCIATED CONTENT

Ⓢ Supporting Information

Experimental protocols, resistivity, and electrochemical analysis are provided. This material is available free of charge via the Internet at http://pubs.acs.org.

■ AUTHOR INFORMATION

Corresponding Author

jaiz@seas.harvard.edu; bjkaehr@sandia.gov

Notes

The authors declare no competing financial interest.

■ ACKNOWLEDGMENTS

■ REFERENCES

(1) Chen, A.; Holt-Hindle, P. *Chem. Rev.* **2010**, *110*, 3767.

(2) Mark, D.; Haeberle, S.; Roth, G.; Von Stetten, F.; Zengerle, R. *Chem. Soc. Rev.* **2010**, *39*, 1153.

(3) Liao, Y.; Song, J.; Li, E.; Luo, Y.; Shen, Y.; Chen, D.; Cheng, Y.; Xu, Z.; Sugioka, K.; Midorikawa, K. *Lab Chip* **2012**, *12*, 746.

(4) Ke, K.; Hasselbrink, E. F. Jr; Hunt, A. J. *Anal. Chem.* **2005**, *77*, 5083.

(5) Paxton, W. F.; Sundararajan, S.; Mallouk, T. E.; Sen, A. *Angew. Chem., Int. Ed.* **2006**, *45*, 5420.

(6) Wang, J. *ACS Nano* **2009**, *3*, 4.

(7) Mei, Y.; Solovev, A. A.; Sanchez, S.; Schmidt, O. G. *Chem. Soc. Rev.* **2011**, *40*, 2109.

(8) Iles, A.; Habgood, M.; de Mello, A. J.; Wootton, R. C. R. *Catal. Lett.* **2007**, *114*, 71.

(9) Urakawa, A.; Trachsel, F.; von Rohr, P. R.; Baiker, A. *Analyst* **2008**, *133*, 1352.

(10) Xu, B.-B.; Zhang, R.; Liu, X.-Q.; Wang, H.; Zhang, Y.-L.; Jiang, H.-B.; Wang, L.; Ma, Z.-C.; Ku, J.-F.; Xiao, F.-S.; Sun, H.-B. *Chem. Commun.* **2012**, *48*, 1680.

(11) Kaehr, B.; Shear, J. B. *J. Am. Chem. Soc.* **2007**, *129*, 1904.

(12) Nielson, R.; Kaehr, B.; Shear, J. B. *Small* **2009**, *5*, 120.

(13) Ismagilov, R. F.; Schwartz, A.; Bowden, N.; Whitesides, G. M. *Angew. Chem.* **2002**, *114*, 674.

(14) Paxton, W. F.; Kistler, K. C.; Olmeda, C. C.; Sen, A.; Angelo, S. K. S.; Cao, Y.; Mallouk, T. E.; Lammert, P. E.; Crespi, V. H. *J. Am. Chem. Soc.* **2004**, *126*, 13424.

(15) Kline, T. R.; Paxton, W. F.; Wang, Y.; Velegol, D.; Mallouk, T. E.; Sen, A. *J. Am. Chem. Soc.* **2005**, *127*, 17150.

(16) Solovev, A. A.; Mei, Y.; Ureña, E. B; Huang, G.; Schmidt, O. G. *Small* **2009**, *5*, 1688.

(17) Solovev, A. A.; Sanchez, S.; Meiz, Y.; Schmidt, O. G. *Phys. Chem. Chem. Phys.* **2011**, *13*, 10131.

(18) Tanaka, T.; Ishikawa, A.; Kawata, S. *Appl. Phys. Lett.* **2006**, *88*, 081107.

(19) Ishikawa, A.; Tanaka, T.; Kawata, S. *Appl. Phys. Lett.* **2006**, *89*, 113102.

(20) Xu, B.-B.; Xia, H.; Niu, L.-G.; Zhang, Y.-L.; Sun, K.; Chen, Q.-D.; Xu, Y.; Lv, Z.-Q.; Li, Z.-H.; Misawa, H.; Sun, H.-B. *Small* **2010**, *6*, 1762.

(21) Maruo, S.; Saeki, T. *Optics Express* **2008**, *16*, 1174.

(22) Allen, R.; Nielson, R.; Wise, D. D.; Shear, J. B. *Anal. Chem.* **2005**, *77*, 5089.

(23) Einaga, H.; Harada, M. *Langmuir* **2005**, *21*, 2578.

(24) Bai, L.; Zhu, H.; Thrasher, J. S.; Street, S. C. *ACS Appl. Mater. Interfaces* **2009**, *1*, 2304.

(25) Harada, M.; Saijo, K.; Sakamoto, N. *Colloids Surf., A* **2009**, *349*, 176.

(26) Sakamoto, Y.; Fukuoka, A.; Higuchi, T.; Shimomura, N.; Inagaki, S.; Ichikawa, M. *J. Phys. Chem. B* **2004**, *108*, 853.

(27) Ware, M. *J. Photogr. Sci.* **1986**, *34*, 165.

(28) Jiang, J.; Hall, T. D.; Tsagalas, L.; Hill, D. A.; Miller, A. E. *J. Power Sources* **2006**, *162*, 977.

(29) Jiang, J.; Miller, A. E. *J. Power Sources* **2007**, *173*, 867.

(30) Porter, G. B.; Doering, J. G. W.; Karanka, S. *J. Am. Chem. Soc.* **1962**, *84*, 4027.

(31) Chen, J.; Zhang, H.; Tomov, I. V.; Rentzepis, P. M. *Inorg. Chem.* **2008**, *47*, 2024.

(32) Cao, Y.-Y.; Takeyasu, N.; Tanaka, T.; Duan, X.-M.; Kawata, S. *Small* **2009**, *5*, 1144.

(33) Kaneko, K.; Sun, H.-B. *Appl. Phys. Lett.* **2003**, *83*, 1426.

(34) LaFratta, C. N.; Fourkas, J. T.; Baldacchini, T.; Farrer, R. A. *Angew. Chem., Int. Ed.* **2007**, *46*, 6238.

(35) Cahill, D. G. *Rev. Sci. Instrum.* **2004**, *75*, 5119.

(36) *Ted Pella, Inc.*; http://tedpella.com/, (accessed November 1, 2011).

(37) Dollimore, D. *Thermochim. Acta* **1987**, *117*, 331.

(38) Gallagher, P. K.; Kurkjian, C. R. *Inorg. Chem.* **1966**, *5*, 214.

(39) The discrepancy between minimum line width and laser spot size (∼700 nm) is attributed to heating at the laser focal point, as discussed, which degrades resolution by increasing the size of the effective volume where precursors are reduced.

(40) Paxton, W. F.; Baker, P. T.; Kline, T. R.; Wang, Y.; Mallouk, T. E.; Sen, A. *J. Am. Chem. Soc.* **2006**, *128*, 14881.

(41) Kaehr, B.; Brinker, C. J. *Chem. Commun.* **2010**, *46*, 5268.

(42) Khripin, C. Y.; Pristinski, D.; Dunphy, D. R.; Brinker, C. J.; Kaehr, B. *ACS Nano* **2011**, *5*, 1401.

(43) Zhang, Y.-L.; Chen, Q.-D.; Xia, H.; Sun, H.-B. *Nano Today* **2010**, *5*, 435.

(44) Cao, Y.-Y.; Dong, X.-Z.; Takeyasu, N.; Tanaka, T.; Zhao, Z.-S.; Duan, X.-M.; Kawata, S. *Appl. Phys. A: Mater. Sci. Process.* **2009**, *96*, 453.

(45) Soleymani, L.; Fang, Z.; Sargent, E. H.; Kelley, S. O. *Nat. Nanotechnol.* **2009**, *4*, 844.